Stacked long Josephson junctions in zero magnetic field: A numerical study of coupled one-dimensional sine-Gordon equations

R. Kleiner,[1] T. Gaber,[2] and G. Hechtfischer[2,*]
[1]*Physikalisches Institut-Experimentalphysik II, Universität Tübingen, Auf der Morgenstelle 14, D-72076 Tübingen, Germany*
[2]*Physikalisches Institut III, Universität Erlangen-Nürnberg, D-91058 Erlangen, Germany*
(Received 29 November 1999; revised manuscript received 18 April 2000)

We present a systematic numerical study of the coupled one-dimensional sine-Gordon equations for a stack of 20 Josephson junctions, with junction parameters that are representative for intrinsic Josephson junctions in $Bi_2SrCa_2Cu_2O_8$. Simulations were performed for zero external magnetic field. We found a large variety of fluxon and antifluxon modes, often involving the excitation of collective Josephson plasma oscillations or cavity resonances. Representative states are discussed in detail.

I. INTRODUCTION

The dynamics of stacked long Josephson junctions has attracted considerable interest for several reasons. For example, vertical stacking of Josephson junctions offers the possibility of realizing efficient high-frequency oscillators or mixers;[1,2] understanding their internal dynamics will be essential for a proper device design. From a more basic point of view, stacked long Josephson junctions provide a well-defined system to investigate nonlinear dynamics. Even a single long junction is known to exhibit a rich variety of dynamical states resulting from the solitonic nature of Josephson flux quanta.[3,4] Coupling Josephson junctions by stacking leads to nontrivial new dynamic effects like Cherenkov radiation by Josephson fluxons which has been seen both in low-T_c (Ref. 5) and in high-T_c stacked junctions;[6] without doubt a large variety of effects is still to be discovered.

Stacked junctions can be realized relatively easy. In Nb technology, artificial stacks of up to 10 (Refs. 3 and 7) or even as much as 28 junctions have been made.[8] Moreover, the most anisotropic high-temperature superconductors like $Bi_2SrCa_2Cu_2O_8$ (BSCCO) or $Tl_2Ba_2Ca_2Cu_3O_{10}$ (TBCCO) intrinsically provide Josephson junction stacks.[9] Here, the interlayer supercurrent flowing between adjacent CuO_2 bi- or trilayers has turned out to be of the Josephson type. Adequately prepared structures like mesas on top of BSCCO single crystals[10] or step structures patterned from BSCCO whiskers[11] or TBCCO thin films[12] naturally form atomically spaced stacks of up to several hundred junctions. It has turned out that for these junctions the Josephson length determining the size of a Josephson vortex is 1 μm or even smaller. Almost all experiments performed so far have been made with stacks much larger in size. A proper discussion thus has to incorporate the finite length of the junctions.

The equations describing the dynamics of stacked long Josephson junctions are the coupled sine-Gordon equations. They can be derived from the Lawrence-Doniach model[13] of layered superconductors.[14–17] In the framework of artificially made, say Nb/Al-AlO_x/Nb, Josephson junctions the coupled sine-Gordon equations have been worked out by Sakai, Bodin, and Pedersen.[18] The (inductive) interaction between adjacent junctions is due to supercurrents flowing along the superconducting layers. If the layer thickness is well below the London penetration depth the supercurrent flowing along a given layer is felt by both junctions sharing this layer. The model is also assumed to be adequate for intrinsic junction stacks in high-temperature superconductors. Here, the thickness of the superconducting layers (i.e., the CuO_2 layers) is only about 3 Å resulting in a enormously strong inductive coupling.[19] There are other possible coupling mechanisms for intrinsic junction stacks, e.g., capacitive interactions[20] or nonequilibrium effects.[21] However, the interaction via these terms seems to be weak, although it should be addressed in situations where current flow along the layers is absent.[22] Particularly in the presence of a magnetic-field-oriented parallel to the layers the coupled sine-Gordon equations provided a good description of the experiments.[19,23–29]

While the coupled sine-Gordon equations have been studied extensively for two-junction stacks,[3] for stacks consisting of more junctions only some special cases have been analyzed, like the dispersion laws of small amplitude linear waves,[17,30–32] the resonant motion of Josephson fluxons in large magnetic fields[33] or some specific fluxon configurations.[14–16,34–36] Numerical treatments of more than two junctions has been limited to specific situations simply because of the lack of sufficient computing power.[3,6,19,23,29,37–39] With present day computers, however, systems of some ten junctions can be investigated on reasonable time scales.

The intention of this paper is to discuss the dynamic states obtained in numerical simulations of the one-dimensional coupled sine-Gordon equations for a 20-junction stack in zero magnetic field as systematically as possible. A discussion of solutions in external magnetic fields oriented parallel to the layers will be given elsewhere.[40] We use parameters that are typical for intrinsic Josephson junctions in BSCCO. The calculations have been performed for a 10 μm long stack. The width of the stack is neglected.

II. COUPLED SINE-GORDON EQUATIONS

The geometry of N stacked long Josephson junctions is shown in Fig. 1. $N+1$ superconducting layers of thickness d are separated by insulating layers of thickness $\bar{t}$. Superconducting layers are labeled from 0 to N, insulating layers from 0 to $N-1$. A bias current with homogeneous density $j_{\rm ext}$ is

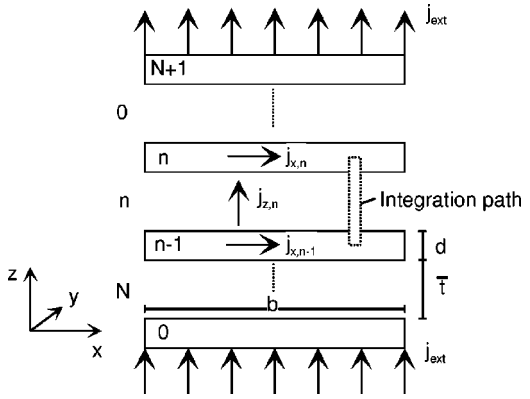

FIG. 1. Geometry of a stack of N long Josephson junctions.

injected into layer 0 and is extracted from layer N. The in-plane London penetration depth into each superconducting layer is λ_L. The length of the stack along x is b; its width along y is neglected. The nth Josephson junction is formed by the superconducting layers $n-1$ and n and the insulating layer in between; the current density across this junction is represented by

$$j_{z,n}=j_{c,n}\sin\gamma_n+E_{z,n}/\rho_n+\epsilon\epsilon_0\dot{E}_{z,n}. \tag{1}$$

The first term on the right-hand side represents the Josephson current density with critical current density j_{cn} and the gauge-invariant phase difference

$$\gamma_n=\varphi_n-\varphi_{n-1}-\frac{2e}{\hbar}\int_{(n-1)(\bar{t}+d)}^{n(\bar{t}+d)}A_z dz; \tag{2}$$

φ_n denotes the phase of the order parameter in the nth superconducting layer; A_z is the z component of the vector potential. The second and third term on the right-hand side of Eq. (1) represent the (linearized) quasiparticle current and the displacement current. Assuming, for simplicity, identical junction parameters, with the use of the Josephson relation $\dot{\gamma}_n=2eU_n/\hbar=2\pi E_{z,n}\bar{t}/\Phi_0$ and the use of normalized time, $\tau=t\cdot 2\pi j_c\rho\bar{t}/\Phi_0$, and electrical field, $e_z=E_z/(j_c\rho)$, Eq. (1) may be written as

$$\frac{j_{z,n}}{j_c}=\sin\gamma_n+\dot{\gamma}_n+\beta_c\ddot{\gamma}_n, \tag{3}$$

with the McCumber parameter $\beta_c=2\pi j_c\rho^2\epsilon\epsilon_0\bar{t}/\Phi_0$. The density of the supercurrent flowing along the nth superconducting layer is denoted $j_{x,n}$. Assuming the amplitude of the order parameter in the superconducing layers to be constant the phase gradient in each layer along x is given by $\partial\phi/\partial x=2e/\hbar\cdot(A_{x,n}+\mu_0\lambda_L^2 j_{x,n})$. Integration of the phase gradient along the contour shown in Fig. 1 yields

$$\frac{\partial\gamma_n}{\partial x}=\frac{2e}{\hbar}\left(\frac{\partial}{\partial x}\oint_C\vec{A}d\vec{s}+\mu_0\lambda_L^2\cdot(j_{x,n}-j_{x,n-1})\right). \tag{4}$$

Assuming an exponential decay of the magnetic field $B_{s,n}$ inside the nth superconducting layer,

$$B_{s,n}=\frac{B_n+B_{n+1}}{2}\frac{\cosh(z/\lambda_L)}{\cosh(d/2\lambda_L)}+\frac{B_{n+1}-B_n}{2}\frac{\sinh(z/\lambda_L)}{\sinh(d/2\lambda_L)}, \tag{5}$$

where B_n denotes the field in the nth insulating layer, one finds with the use of Maxwell's equations:

$$\frac{\partial^2\gamma_n}{\partial x^2}\equiv\gamma_n''=\frac{1}{\lambda_m^2}\frac{j_{z,n}}{j_c}+\frac{1}{\lambda_k^2}\frac{2j_{z,n}-j_{z,n-1}-j_{z,n+1}}{j_c}, \tag{6}$$

where the lengths λ_m and λ_k are given by $\lambda_m=[\Phi_0/(2\pi j_c\mu_0 t_{\rm eff})]^{1/2}$ and $\lambda_k=[\Phi_0 d_{\rm eff}/(2\pi j_c\mu_0\lambda_L^2)]^{1/2}$, with $t_{\rm eff}=\bar{t}+2\lambda_L\tanh(d/2\lambda_L)$ and $d_{\rm eff}=\lambda_L\sinh(d/2\lambda_L)$. In the limit $d,\bar{t}\ll\lambda_L$, which is clearly fulfilled for intrinsic junctions with $d\approx 3$ Å, $\bar{t}\approx 12$ Å, and $\lambda_L\approx 1500$ Å, $t_{\rm eff}$ and $d_{\rm eff}$ reduce to $t_{\rm eff}=\bar{t}+d$ and $d_{\rm eff}=d$. Equations (6) and (3) form the basis of the dynamic description of stacked long Josephson junctions.[18] For the inner- and outermost junctions, respectively, the terms $j_{z,n-1}$ and $j_{z,n+1}$, have to be replaced by $j_{\rm ext}$. If no currents leave the stack at its left and right edges, from Eq. (4) the boundary condition

$$\gamma_n'(x=0)=\gamma_n'(x=b)=\frac{2e}{\hbar}B_{\rm ext}t_{\rm eff}=0 \tag{7}$$

can be derived. Here, self-fields due to currents flowing along z have been neglected. Introducing the vectors $\vec{\gamma}=(\gamma_1,\ldots,\gamma_N)$ and $\vec{j}_z=(j_{z,1},\ldots,j_{z,N})$, Eq. (6) can be written as

$$\vec{\gamma}=M\frac{\vec{j}_z}{j_c}-\frac{1}{\lambda_k^2}(1,0,\ldots,0,1)\frac{j_{\rm ext}}{j_c} \tag{8}$$

or, equivalently,

$$\vec{\gamma}''-\frac{1}{\lambda_m^2}\frac{j_{\rm ext}}{j_c}\cdot\vec{1}=M\cdot\frac{\vec{j}_z-\vec{j}_{\rm ext}}{j_c}, \tag{9}$$

with $\vec{1}=(1,1,\ldots,1)$. The elements $M_{i,k}$ of the matrix M are given by $M_{i,i}=\lambda_m^{-2}+2\lambda_k^{-2}\equiv\lambda_j^{-2}$, $M_{i,i+1}=M_{i-1,i}=-\lambda_k^{-2}$, and $M_{i,k}=0$ otherwise. For a numerical solution we transformed the partial differential equations (9) into a set of ordinary differential equations in time using the multimode expansion[19]

$$\gamma_n(x,t)=\gamma_{n,0}(t)-\sum_{k=1}^{K}\gamma_{n,k}(t)\cos\left(\pi\frac{x}{b}x\right) \tag{10}$$

involving $(K+1)$ Fourier components $\gamma_{n,k}$. Note that Eq. (10) automatically fulfills the boundary conditions, Eq. (7). We solve the resulting ordinary differential equations using a fifth-order Runge-Kutta method. For the calculations discussed below we either used $K=32$ or $K=64$. The calculations are for a 20 junction stack with a length $b=10$ μm. Unless stated otherwise all junctions had identical parameters. The critical current density was 1000 Å/cm^2, a typical value for intrinsic Josephson junctions. We used $\lambda_L=1500$ Å, $d\approx d_{\rm eff}=3$ Å, and $\bar{t}=12$ Å, corresponding to $\lambda_m\approx 132$ μm, $\lambda_k\approx 0.59$ μm, $\lambda_j\approx 0.42$ μm, and $t_{\rm eff}=15$ Å. We thus work in a limit where the lateral stack

dimensions are much smaller than λ_m, and the stack thickness is well below λ_L. The ratio b/λ_j, on the other hand is large, about 24. For the McCumber parameter we used $\beta_c = 50$. A value of 10^4 would have been more realistic for intrinsic Josephson junctions. However, for β_c values that large simulations would have been by far too much time consuming.

III. DYNAMIC SOLUTIONS IN ZERO MAGNETIC FIELD

We now turn to dynamic solutions obtained for the 20 junction stack for nonzero bias currents in the absence of external magnetic fields. Basically, there are three different dynamic states—motion of fluxons or antifluxons, collective small amplitude oscillations of the phases $\gamma_n(x,t)$ (collective plasma oscillations), and resistive (McCumber) states where the phases $\gamma_n(x,t)$ evolve almost linearly in time. For a Josephson junction stack the interplay between these states leads to a rich variety of dynamic solutions; some of them will be discussed below. We will first briefly review the collective Josephson-plasma modes and continue with a discussion of states involving the motion of a single Josephson fluxon. We will then turn to the full current-voltage characteristics and more complex fluxon modes.

Collective plasma oscillations

The coupled sine-Gordon equations allow for collective small amplitude oscillations of the phases $\gamma_n(x,t)$ of the form

$$\gamma_n(x,t) = g_1 + g_2 \sin(\omega_{qk} t) \sin\left(\pi \frac{(n+1)q}{N+1}\right) \cos\left(\pi \frac{kx}{b}\right) \tag{11}$$

with some amplitudes g_1 and g_2.[17,31,33] The wave number k in the x direction can take integer values 0,1, . . . , and the wave number q in the z direction runs from 1 to N. The frequencies ω_{qk} are given by

$$\omega_{qk}^2 = \omega_{pl}^2 (1 - I/I_c)^2 + c_q^2 (\pi k/b)^2, \tag{12}$$

where $\omega_{pl} = [2\pi \bar{t} j_c/(\Phi_0 \epsilon \epsilon_0)]^{1/2}$ is the Josephson plasma frequency. The velocities c_q are given by

$$c_q = \frac{\omega_{pl} \lambda_J}{\sqrt{1 - 2s \cos \pi q/(N+1)}}; \tag{13}$$

$s = (\lambda_k/\lambda_J)^2$ denotes the coupling parameter[18] which equals 0.499 995 for the parameters used. For $N=1$, c_q reduces to the Swihart velocitiy $\bar{c} = \omega_{pl} \lambda_j$. For intrinsic Josephson junctions, the plasma frequency f_{pl} ranges between 100 and 300 GHz,[2] and $\bar{c}$ is on the order of 10^5 m/s.[23]

The electric field ($\propto \dot{\gamma}_n$) created by the plasma oscillations corresponds to a two-dimensional standing wave pattern with k and q counting the half waves along x and z, respectively.[33] We denote this cavity resonance (q/k). The electric-field amplitude in each junction is maximum at the edges of the stack at $x=0$ and $x=b$. For $\sin \omega_{qk} t = 1$, the electric fields $E_{z,n}(x=0)$, when plotted vs n, are located on a sinusoidal curve with q half-waves along z. The outermost nodes are located one junction position *outside* the stack. Consequently, for an $(1/k)$ resonance, the maximum amplitude of the electric field across a junction increases towards the center junctions. For $(2/k)$ resonances there is a node in the center of the stack, and for (N/k) resonances the electric field across adjacent junctions alternates, but again with increasing amplitude towards the center of the stack. Note that, particularly for q values between N and $N/2$, the electric-field amplitudes across adjacent junctions may form complicated patterns whenever the junction number and the period along z, $q/(N+1)$ are not commensurable.

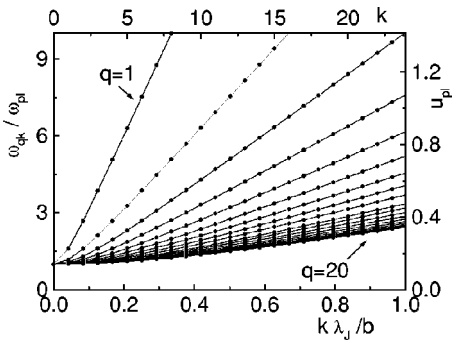

FIG. 2. Dispersion of the collective Josephson plasma frequencies ω_{qk} vs k. Values for fixed q are connected by lines. The right-hand axis shows the corresponding normalized voltage, $u_{pl} = U_{pl}/(I_c R) = \omega_{qk}/(\omega_{pl} \beta_c^{1/2})$. For β_c, a value of 50 has been used to calculate u_{pl}.

Figure 2 shows the dispersion of ω_{qk} vs k for zero bias current for the 20 junction stack used for the calculations. Allowed values of k are marked by dots. Almost all curves concentrate close to the limiting curve $\omega_{qk} = \omega_{pl}(1 + (\pi \lambda_j/b)^2 k^2/2)^{1/2}$ that would be obtained for large values of N and q. Using the Josephson frequency-voltage relation, the frequencies ω_{qk} can be transferred into the normalized voltage $u_{pl} = U_{pl}/(I_c R) = \omega_{qk}/(\omega_{pl} \beta_c^{1/2})$ (right-hand axis of Fig. 2) useful for a comparison to the current-voltage characteristics discussed below.

For the dynamics of stacked junctions the frequencies ω_{qk} play a twofold role. First, the collective cavity resonances can be excited by the ac Josephson currents leading to resonant structures in the current-voltage characteristics. Second, in stacked junctions the maximum fluxon velocity can be larger than the phase velocity $\omega_{qk}/(\pi k/b)$ of some of the plasma modes leading to a strong coupling of fluxons and plasma waves by the Cherenkov mechanism.[5,6]

Single fluxon states

The most simple fluxon state of a single long Josephson junction in zero magnetic field is the motion of a single fluxon being reflected at the junction edges. Its maximum velocity is the Swihart velocity $\bar{c} = \omega_{pl} \lambda_J$. In the current-voltage characteristic this state shows up as a zero field step with a limiting voltage given by $V_L = \Phi_0 \bar{c}/b$, or $v_L = 2\pi \lambda_J/(\beta_c^{1/2} b)$ in dimensionless units. Note that $\bar{c}$ is also the minimum phase velocity of plasma waves in the junction. Consequently, plasma and fluxon modes are well separated and Cherenkov radiation does not occur. For the parameters used, $v_L = 0.038$. In a stack of junctions it is *a priori* not clear what the maximum velocity of a fluxon is. If the value is close to $\bar{c}$ the vortex can exceed the minimum phase velocities c_q of the plasma modes for q values between $N/2$ and N.

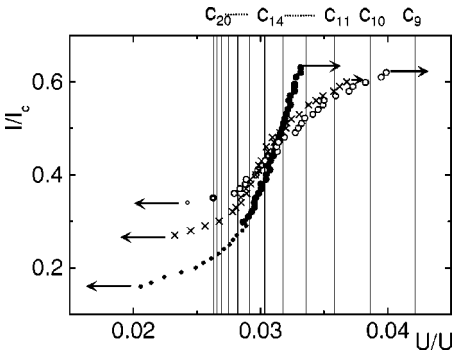

FIG. 3. Zero-field step with one vortex either in junction 0 (closed circles), 1 (crosses) or in 10 (open circles). Vertical lines correspond to phase velocities $c_q = \omega_{qk}/(\pi k/b)$ for $q = 9$ to 20.

For the simulations we placed a fluxon into one of the junctions of the stack at a bias current of $i = 0.4$. The fluxon was introduced as a static one located at $x = 0.5$. Under the drive of the bias current it accelerated and got reflected at the junction edges. The voltage across the stack was integrated until its time-averaged value was defined better than 10^{-3}. Then the bias current was increased by steps of 0.01. Each time the system evolved to another steady state the bias current was changed in steps of 0.01. Figure 3 shows results for the first zero-field step with the fluxon located, respectively, in the outermost junction 0, in junction 1, and in the innermost junction 10. When the vortex moved through the outermost junction the zero-field step was stable between $i = 0.16$ and $i = 0.63$. For bias currents larger than $i = 0.22$ the fluxon velocity exceeded the lowest phase velocity c_{20} of the plasma waves. The single-vortex configuration became unstable when the vortex velocity approached c_{12}. Note that the zero-field step never gets vertical as it would be the case for a single long Josephson junction. Here, the limiting Swihart velocity would correspond to a normalized voltage of 0.037 which is between c_{10} and c_{11}. Also, for a single junction the vortex would have been stable up to a bias current of almost 1.

With the vortex oscillating in junction 1 we found a smaller stability range $0.27 < i < 0.6$. The maximum vortex velocity, however, was larger than c_{11}. Finally, when the vortex was oscillating in junction 10, the zero-field step was stable for vortex velocities above c_{20}, and a maximum velocity larger than c_{10} could be achieved. However, the zero-field step obtained here is not much different from the latter case indicating that boundary effects are restricted mostly to the outermost layer.

Figure 4 shows snapshots of the supercurrent distribution in the stack with the vortex oscillating in junction 0 for $i = 0.18$ (a), i.e., for a vortex velocity below c_{20}, and for $i = 0.6$ (b), i.e., for a vortex velocity above c_{13}. In the first case the shape of the vortex is similar to the single junction case whereas in the latter case trailing plasma waves are excited. This effect has been discussed by Goldobin *et al.*[5] and by Hechtfischer *et al.*[6] based on simulations of a seven-junction stack with periodic boundary conditions. A discussion of the fluxon shape for a double junction stack has been given by Krasnov *et al.*[41]

Figure 5 shows a similar snapshot with the vortex oscillating in junction No. 10 for a bias current close to the lower

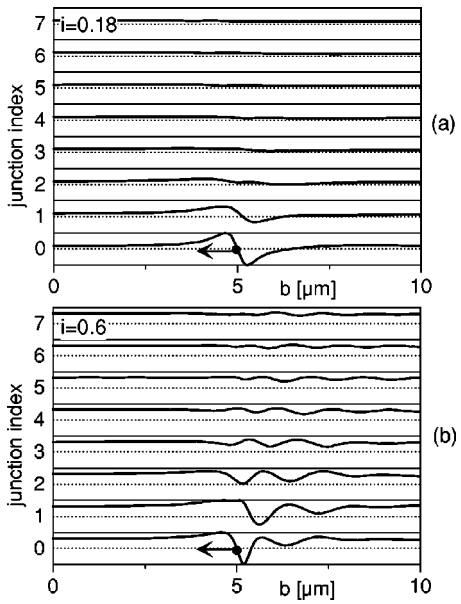

FIG. 4. Snapshot of single fluxon oscillating in junction 0 at bias currents of $i = 0.18$ (a) and 0.6. (b) At $i = 0.18$ the fluxon velocity is below the lowest phase velocity of plasma waves whereas at $i = 0.6$ the fluxon is faster than phase velocities for $q = 20$ to 13. Centers of Josephson vortices are marked by circles; lines show distribution of Josephson currents; lines are vertically offset to map the geometry of the stack. Only junctions 0–7 are shown.

end of the zero-field step. The vortex velocity is just above c_{20} and the trailing wave just starts to establish with a relatively large value of k.

Figure 6 shows the vortex at $i = 0.56$. Its velocity is above c_{12}. The figure displays three subsequent shapshots when the vortex is near the left edge of the junction. At the top figure the vortex approaches the junction edge. Note that the trailing waves have much larger wavelengths than in Fig. 5. This occurs because, with increasing velocity, the vortex velocity matches the phase velocity ω_{qk}/k at successively smaller values of k. In contrast to the single junction case or the case of low vortex velocities in the stack, the vortex is not simply reflected at the edge. Instead, it first disappears from the stack. A short time later, a fluxon-antifluxon pair is created near the left edge; the antifluxon moves to the right whereas the fluxon leaves the stack. For a short time, another antifluxon appears in junction 9, however gets annihilated at the boundary before moving to the right.

When the bias current was increased to values above 0.62, vortices were created in junctions 9 and 11, similar to the

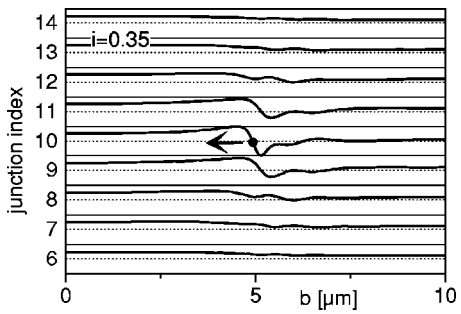

FIG. 5. Snapshot of single fluxon oscillating in junction 10 at a bias current of $i = 0.35$. Only junctions 6 to 14 are shown.

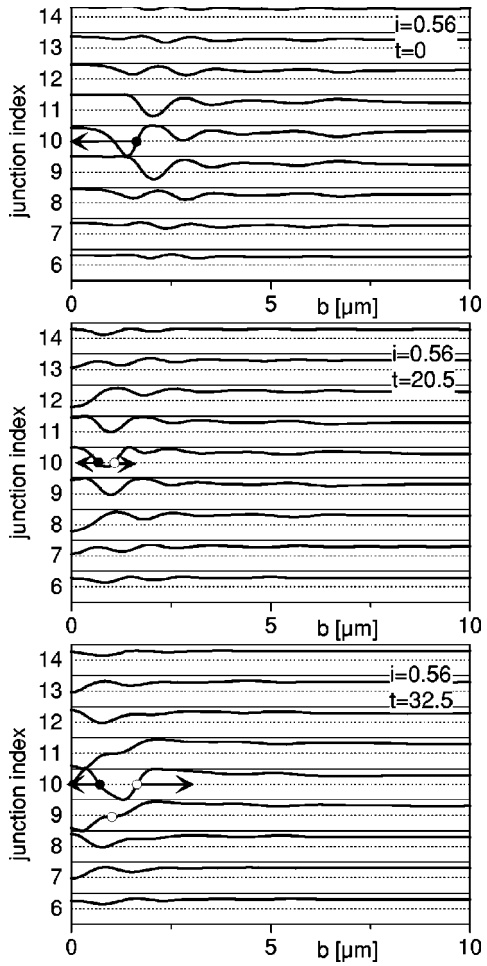

FIG. 6. Three snapshots of single fluxon moving in junction 10 at a bias current of $i=0.55$. At $t=0$ the fluxon approaches the left boundary and drops out of the junction (top). After some time units a fluxon-antifluxon pair is created near the left edge (middle). The antifluxon (open circle) continues to move towards the right edge whereas the fluxon drops out of junction 10. Another antifluxon appears in junction 9 (bottom) but gets annihilated by a fluxon a few time units later. Time is given in units of $2\pi\Phi_0/I_cR$. Only junctions 6–14 are shown.

case of Fig. 6. However, they did not drop out of the system but started to oscillate in these junctions creating even more vortex-antivortex pairs when approaching the boundaries. This transient situation stabilized when junctions 6 to 14 had switched to the resistive state; one vortex oscillated in junction 5 and another one in junction 15. A similar scenario was found with the vortex initially oscillating in junction 0 where, finally, junctions no. 0 to 5 switched to the resistive state.

The above simulations have been performed with one fluxon in one of the junctions while all other junctions were in the superconducting (i.e., zero dc voltage) state. Another situation—unique to stacks—is to have one vortex in one junction, while some of the other junctions are in the resistive state. Figure 7(a) shows a situation for $i=0.75$ where the vortex is located in junction 10. Junctions 9 and 11 are in the resistive state, and all other junctions are in the superconducting state. When the fluxon in junction 10 moves to the left one antifluxon in junction 9 and one antifluxon in junction 11 enter rapidly, get slowed down near the fluxon in

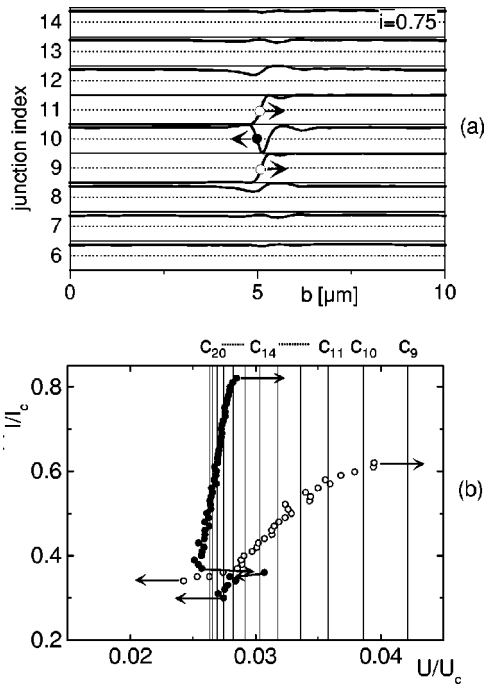

FIG. 7. (a) Snapshot of current distribution for a single vortex moving in junction 10 at $i=0.75$; junctions 9 and 11 are in the resistive state. Only junctions 6–14 are shown. (b) Bias current vs dc voltage across junction 10. Solid markers: single vortex in junction 10; junctions 9 and 11 in the resistive state. Open markers: single vortex in junction 10, all other junctions in the superconducting state. Vertical lines correspond to phase velocities $c_q=\omega_{qk}/(\pi k/b)$ for $q=9-20$.

junction 10 and leave rapidly after they have passed this vortex. The process occurrs very often during one cycle of the vortex in junction 10. Initially, junctions 9 and 11 have been oscillating with random relative phases; the configuration of Fig. 7(a) established after a short period of time. The time-averaged voltage obtained was 0.747 for junctions 9 and 11, and 0.027 for the vortex in junction 10. Figure 7(b) shows the bias current vs dc voltage across junction 10 for this state (solid markers) in comparison to the situation when junctions 9 and 10 are in the superconducting state (cf. Fig. 3). Apparently, the vortex oscillating in junction 10 is slowed down by the resistive junctions 9 and 11. A similar effect has been recently observed in experiment and simulations of a two-layer system.[42] However, the range of stability of this mode is enhanced reaching a maximum bias current above 0.8.

When the bias current was decreased to 0.36, junctions 9 and 11 switched to the superconducting state. A standing electric-field wave pattern with $k=10$ developed in this case leading to an *increased* voltage drop across junction 10. When the bias current was further decreased by 0.01 this pattern was replaced by 6 vortices oscillating in junction 9, and four vortices oscillating in junction 11. Here, the dc voltage across junction 10 jumped towards smaller values [cf. arrows in Fig. 7(b)]. This configuration remained stable until the system switched back to the zero voltage state.

McCumber branches

When ramping up the bias current from zero, the stack stays in the superconducting state with homogeneous supercurrent distribution until the critical current is reached. Since

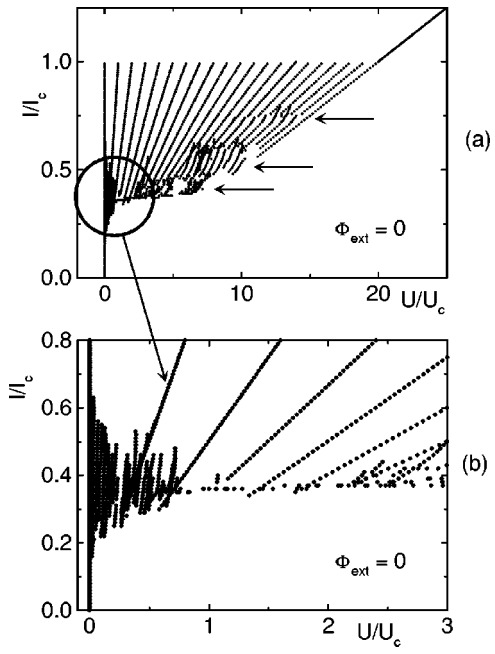

FIG. 8. Current-voltage characteristic of 20 junction stack showing 20 linear resistive branches and a variety of resonant structures and zero-field steps (a). The low voltage region is enlarged in (b).

all junctions are identical they switch to the resistive state (McCumber state) simultaneously. As damping is small ($\beta_c \gg 1$) the phases γ_n increase almost linearly with time leading to a time-averaged voltage across each junction approximately given by $u = U/I_c R = I/I_c = i$. The total voltage across the stack is thus given by $i \approx Nu$. When decreasing the bias current all junctions remain in the McCumber state until some minimum current is reached.

In the absence of spatial variations the junctions are decoupled, as can be seen from Eq. (8). Therefore, in the bias range between the return current and the critical current there are also solutions with n junctions in the superconducting state and $N-n$ junctions in the McCumber state. Every junction can be in any of the two states independent of the others leading to a set of N McCumber branches that differ by the number of resistive junctions. Here, the question arises how to trace out these branches in the simulations. One extremely time consuming way would be to ramp up the bias current from zero until all junctions are resistive, decrease the current until some fluxon state is reached with fluxons in one or a few layers. Another increase of the bias current would lead to states with some junctions being resistive and some others being superconducting. Repeating the procedure many times would eventually yield all possible branches. Another, still time consuming, way would be to add noise to the system, choose a bias current near the critical current and wait until some of the junctions switch to the resistive state. The more easy, although less natural, approach taken by us was to decrease the critical current of one of the junctions for a short time while the bias current was set close to I_c; when this junction had switched to the resistive state the current was decreased in steps of 0.01. In our simulations, a new branch selection criterium was detecting a jump of more than 0.03 units of the voltage across any of the junctions. This branch was then traced both for increasing and decreasing current. The procedure was repeated until zero bias current was

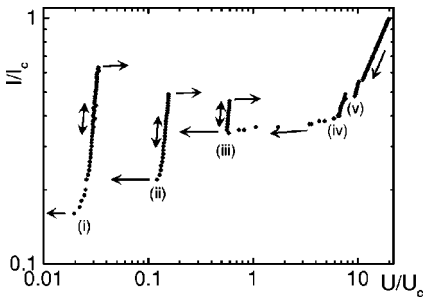

FIG. 9. Current voltage characteristic obtained when all 20 junctions were initially biased in their resistive state. Note the logarithmic current and voltage scales. For a description of branches labeled (i)–(v), see text.

reached. For the simulations shown in Fig. 8 adjacent junctions have been switched to the resistive state one by one starting with junction 1. Relative junction phases were random. The current-voltage characteristic obtained consists of N linear branches corresponding to McCumber states differing by the number of resistive junctions. Note that the nth branch could have been obtained also for many alternative choices of the n resistive junctions within the stack.

When the bias current was decreased below some minimum current the current distribution inside the stack got inhomogeneous leading to the structures in the current-voltage characteristics marked by arrows in Fig. 8(a). These structures are discussed in detail below. Before returning to the superconducting branch a large number of zero-field steps could be obtained [cf. Fig. 8(b)] involving the motion of a few Josephson fluxons in some of the junctions.

Complex fluxon modes

Figure 9 shows a simulation where the stack was initially biased at $i=1$ with all junctions in the resistive state. Junctions were oscillating with the same frequency but with random relative phases. Decreasing the bias current towards zero we essentially found five sub-branches labeled (i)–(v) in Fig. 9. Note the logarithmic scales of this figure. Branch (i) is due to a single vortex oscillating in junction 0. In state (ii) there were two vortices in junction 0, and three vortices in junction 1 oscillating back and forth. Vortices moving in the same direction were well separated, i.e., no bunching occurred. For currents larger than 0.5 junction 1 switched to the resistive state; junction 1 still contained 2 vortices and there was one vortex in junction 2. State (iii) had one vortex in each of the junctions 4, 9, and 11, two vortices in junction 19, three vortices in junction 18, and 8 vortices in junction 1. Between state (iii) and (iv) there was a variety of modes consisting of junctions that had switched to their resisitive states and some others containing oscillating vortices.

States (iv) and (v) are distinctly different from states (i) to (iii). Three snapshots of the supercurrent distribution of state (iv) at $i=0.49$ are shown in Fig. 10. Although each junction contains a large number of vortices and antivortices the overall motion is very regular. At $t=0$ all fluxons are concentrated in the center of the stack; with increasing time fluxons (antifluxons) move to the left (right) forming almost a straight line (cf. Fig. 10, $t=6$). Approximately every second junction is free of vortices. A later snapshot (Fig. 10, $t=11$) shows antifluxons-fluxons returning after reflection at the boundaries. Note that again every second junction is free

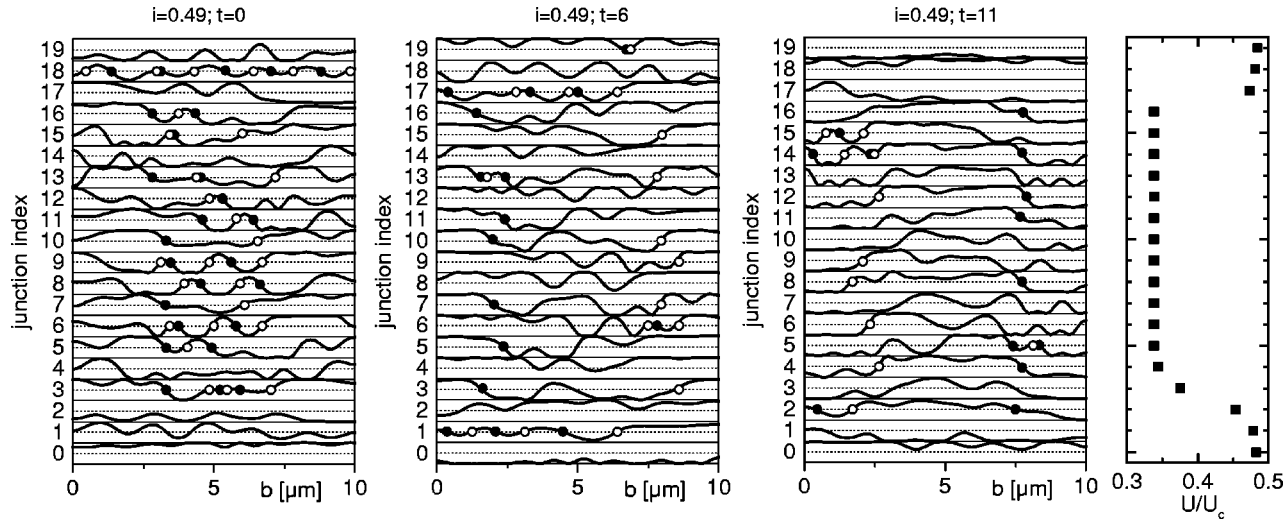

FIG. 10. Three snapshots of supercurrent distribution as obtained for state (iv) of Fig. 9, together with the dc voltage across each junction (right). Fluxon centers are marked by closed circles, centers of antifluxons by open circles. Fluxon motion is towards the left edge, antifluxons move towards the right edge.

of vortices; however positions of junctions carrying vortices have switched by one. The dc voltages across junctions 3–15 are about 0.34 indicating that these junctions were phase locked. The dc voltage across the outermost junctions is about 0.48. Figure 12(a) shows the Fourier transform of the total voltage across the stack. This spectrum and all other spectra shown later are recorded at $x=0$. There is a sharp peak at $f/f_c=0.337$ and some other peaks at frequencies between 0.48 and 0.67, and between 0.16 and 0.19. The electric-field distribution inside the stack showed some indications of a (1/2) standing wave (with $q=1$ and $k=2$), superimposed to the voltage pulses associated with the moving fluxons. According to Eq. (12) the (1/2) resonance should occur at $v=f/f_c=0.35$, which is close to the sharp peak of the Fourier transform of the total voltage. The peak near $f/f_c=0.5$ is apparently due to the unlocked junctions. The peaks at $f/f_c=0.19$ and $f/f_c=0.16$ may arise from higher q resonances, e.g., the (2/2) resonance, to occur at $f/f_c=0.17$, and some mixing product between these frequencies.

Figure 11 shows two snapshots of the supercurrent distribution in the stack for state (v). Two columns of fluxons (antifluxons) and one antifluxon (fluxon) column are clearly visible. Note that, at $t=0$, most fluxons are located in the odd labeled junctions whereas, after reflection at the edges antifluxons appear in the even labeled junction. A similar switching by one junction occurred when the vortex-antivortex columns collided in the middle of the stack. The vortex-antivortex pair in the nth junction annihilated but another pair in the adjacent junction was formed. The electric-field pattern (not shown) exhibited a well developed (1/3) standing wave. Equation (12) yields a dc voltage of 0.53 for this resonance. The voltage drop across the inner junctions 3–17 was 0.5; the voltage across the other junctions was larger. The Fourier transform of the total voltage across the stack [Fig. 12(b)] shows a sharp peak at $f/f_c=0.5$ which can be associated with the (1/3) cavity resonance excited by the fluxons. The peaks located at higher frequencies are caused by the unlocked junctions, while the peak located at $f/f_c=0.037$ seems to be a mixing product of the high-frequency peaks.

Starting with less junctions in the resistive state (cf. Fig. 8) we found, in addition to the resonances discussed above, the (1/4) resonance consisting of four vortex-antivortex columns. This resonance appeared as long as 15 or more junctions were resistive. For small bias currents a variety of states was found consisting of different numbers of vortex-

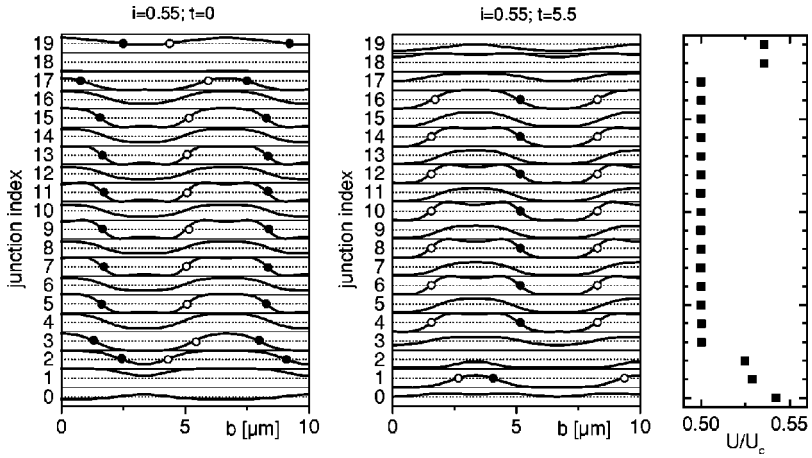

FIG. 11. Two snapshots of supercurrent distribution as obtained for state (v) of Fig. 9, together with the dc voltage across each junction (right). Fluxon centers are marked by closed circles, centers of antifluxons by open circles. Fluxon motion is towards the left edge, antifluxons move towards the right edge.

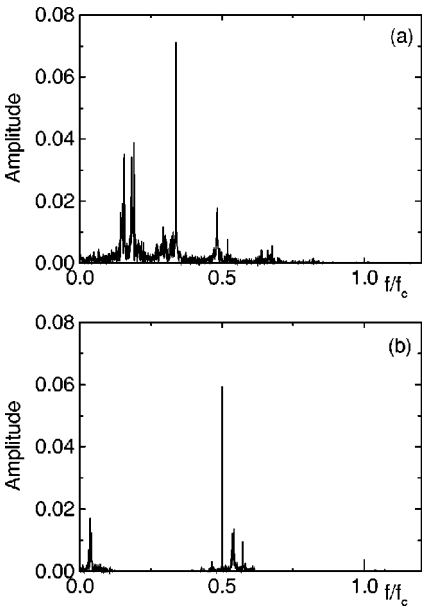

FIG. 12. Fourier transforms of total voltage across the stack taken for (a) state (iv) and (b) state (v) of Fig. 9.

antivortex pairs in various junctions oscillating without an appreciable excitation of cavity resonances [cf. Fig. 8(b)].

Starting with 14 adjacent junctions in the resistive state there was a new state involving the (20/11) resonance as shown in Fig. 13. In the figure, the upper sequence of pictures displays a snapshot at $t=0$ of the current distribution (left) and the electric-field distribution in the stack (middle), in addition to the dc voltage across each junction (right). The snapshot is taken such that the standing wave, as observed in the electric field pattern had a maximum. Here, a relatively small number of vortices is visible. Note that there is no dc voltage across junctions 15–19. The lower row of pictures shows supercurrent and electric-field distribution at $t=7$ where the amplitude of the electric field was almost constant in space. Now a large number of vortex-antivortex pairs is present, and the current distribution varies strongly in space. Figure 14 shows the Fourier transform of the total voltage across the stack. The spectrum is broad, with a maximum around $f/f_c=0.2$. Equation (12), with $q=20$ and $k=11$ yields a normalized Josephson plasma frequency of 0.19 which is close to the observed maximum.

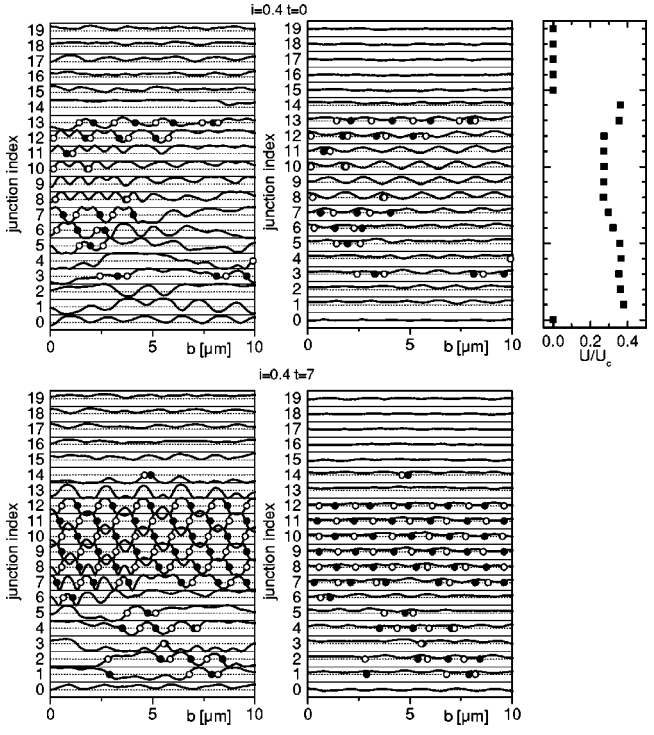

FIG. 13. Upper row: snapshot of supercurrent (left) and electric-field (middle) distribution in the stack involving an antiphase resonance, together with the dc voltage drop across each junction (right). Lower row: snapshot of supercurrent (left) and electric field (middle) distribution in the stack 7 time units later. The (normalized) electric field across the nth junction is vertically offset by the junction index n. Its value is 1 at the upper end of each junction.

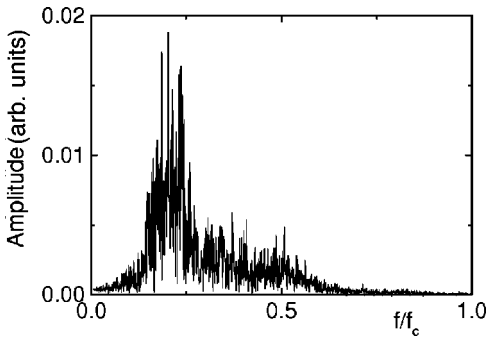

FIG. 14. Fourier transform of total voltage across the stack for the state shown in Fig. 13.

When starting the simulation with less than 14 junctions in the resistive state we found this out of phase mode as long as more than six junctions were resistive. For fewer resistive junctions only states involving the non-resonant motion of vortex-antivortex pairs appeared.

IV. CONCLUSIONS

General considerations

The simulations discussed above have shown that there are at least two classes of structures to be observed in the 20 junction stack in zero magnetic field. One with vortices moving more or less independent, and one involving the excitation of collective cavity resonances with k half-waves along x and q half-waves along z. All states can involve a number of junctions being either in the McCumber or in the superconducting state giving rise to a huge variety of states. For the nonresonant fluxon modes even a large number of vortices within the stack could be stabilized. These modes were clearly favored at low voltages. Even in simple cases with only a few vortices there was a very large variety of different states depending on the precise location of the vortices, their velocity and the state of adjacent junctions. The collective resonances can be ''populated'' with fluxon-antifluxon pairs (cf. Figs. 10–12). They occur at frequencies that are somewhat smaller than given by Eq. (12). This should not be too surprising because Eq. (12) has been derived in the low amplitude limit whereas the resonant states containing vortex-antivortex pairs contain regions where the phases γ_n are large. When more than two thirds of the junctions were initially biased in the resistive state we were able to obtain the

$q=1$ resonant state with small values of k ($k=2$, 3, and 4). The out-of-phase resonance ($q=20$) appeared only if a not too large number of junctions was resistive. We could not find or at least identify other resonances. They may be found in a more detailed search; however the simulations at least indicate that their stability range is not too large.

Stability issues

Although the available computing power was not sufficient to systematically investigate stability of the above states with respect to junction inhomogeneities or thermal noise, at least the stability of some selected states could be studied. As an example we discuss the zero-field (1/3) resonance of Fig. 11. In order to introduce thermal noise we introduced $2K$ independent current noise sources, with a white spectral distribution $4k_BT/R$, for each junction. $K=32$ was the number of Fourier components used. The sources were positioned at equidistant positions along x. In dimensionless units, the spectral noise distribution of each source may be characterized by $\Gamma=2\pi k_BT/(I_c\Phi_0)\equiv I_N/I_c$, similar to noise calculations for superconducting quantum interference devices.[43] $\Gamma^{1/2}$ represents the current noise amplitude in unit bandwidth $\tau=2\pi I_0R/\Phi_0$. For, e.g., a temperature of 77 K I_N is about 3.3 μA. Figure 15 shows the Fourier spectrum of the total voltage across the stack for the zero-field (1/3) resonant mode for—the very huge—noise parameter $\Gamma=0.5$, to be compared with the Fourier transform shown in Fig. 12(b) for the noise-free case. Although the spectrum is broadened, there is still a sharp peak at $f/f_c=0.5$. For this value of Γ still 11 junctions (Nos. 4–14) were locked to the resonance. For comparison, 15 junctions were locked without noise. With $\Gamma=1.0$ there was still a peak at $f/f_c=0.5$ in the Fourier spectrum; six junctions were still locked to the resonance. Also, a 10% scatter in critical current density and resistivity did not affect the resonance strongly. Still, 13 junctions were locked to the resonance demonstrating the robustness of this state.

Comparison to experiment

The final question to be discussed is to what extent the simulations are relevant to the experiment. There is little doubt that artificial, say Nb/Al-AlO_x/Nb, multilayers are described well with the coupled sine-Gordon equations. For intrinsic Josephson junctions, the ideal stack used for the calculations differs by many means from the typical experimental situations. First, most of the mesa structures used in the experiment have lateral dimensions much larger than λ_J. The structures thus should be treated as long both in x and in y direction. At this point one can only speculate about the effect of the the finite width along y. At the very least, it seems clear that the fluxons cannot be considered as rigid along y, most likely causing a decreased stability range of all modes. Second, in the experiment there is no free-standing stack of junctions. Mesa structures are formed on top of a base crystal. The large number of modes that can be excited in the (very large) junctions forming the base crystal are likely to decrease the stability range of collective modes in the mesas. Moreover, the presence of a base crystal breaks the top-bottom symmetry of the stack which is likely to further decrease the stability of at least some of the predicted states. Other stack types like BSCCO whiskers[11] or TBCCO step stacks[12] have ''base crystals'' both on top and at the bottom of the stack. Although the top-bottom symmetry is conserved here, their presence alters the effective magnetic thickness $t_{\rm eff}$ of the outermost junctions. Third, the coupled sine-Gordon equations assume that no pancake vortices penetrating the superconducting layers are present. In many experimental situations these vortices are likely to exist and locally change the spatial dependence of the phases $\gamma_n(x,y)$, providing pinning centers for Josephson fluxons.[44] Finally, the experimental ratio of characteristic frequency and plasma frequency, equal to $\beta_c^{-1/2}$ in Eq. (3), is much larger than its value used in the simulations. Experimental values of f_c and f_{pl} are, respectively, on the order of 10 THz and 150 GHz, corresponding to β_c values of several 10^3. As a consequence, in the experiment, most fluxon states should occur at much smaller voltages (relative to the characteristic voltage) than in the simulations.

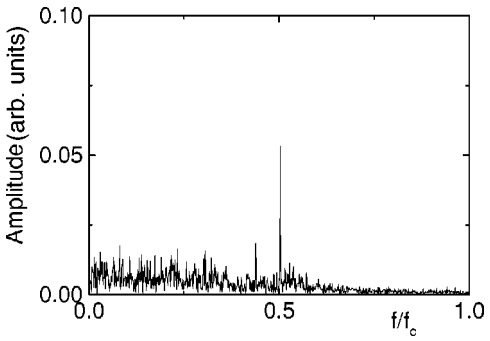

FIG. 15. Fourier transform of the total voltage across the stack for the (1/3) resonance [cf. Figs. 11 and 12(b)] in the presence of thermal noise ($\Gamma=0.5$). The bias current is $i=0.55$.

Which states have been observed? In zero magnetic-field simulations predict a large number of zero-field steps and resonant states. An indication of the existence of fluxon modes in zero field is the multiple-valued critical current,[25] however, to our knowledge, neither zero-field steps nor collective resonances have been observed—except possibly in the presence of external microwave fields,[45] which is beyond the scope of this paper. There are structures on each branch of the current-voltage characteristics which, however, have been identified as resonant interactions with optical phonons.[46–48] The stability of the resonances predicted by the coupled sine-Gordon equations thus seems to be highly reduced. For $f_{pl}=150$ GHz, the (1/5) resonance would, for example, occur at 0.94 THz, which is about the typical lower voltages at which the quasiparticle branches in the experimental current-voltage characteristics are stable. There is, thus, a possibility that in the experiment the stack simply switches back to the superconducting states before the fluxon states can be stabilized. It should, finally, be noted that a number of fluxon and resonant modes, however, have been found in external magnetic fields,[6,19,23–28] although the stability of these modes was clearly less than indicated by the simulations.

It thus seems that at least some of the states predicted by the coupled one-dimensional sine-Gordon equations can be seen in the experiment. The differences between experiment and simulations should not be too surprising since experimentally used mesas differ by many means from the ideal

systems used for the simulations. It seems unclear whether or not intrinsic junction stacks can be realized without a base crystal. However, stacks that are short in y direction are within reach of present day fabrication technologies allowing for more rigorous comparisons between experiment and the model of coupled one-dimensional sine-Gordon equations.

ACKNOWLEDGMENTS

The authors would like to thank A. V. Ustinov and P. Müller for valuable discussions. Financial support by the Bayerische Forschungsstiftung and the Deutsche Forschungsgemeinschaft is greatfully acknowledged.

*Present Address: Rohde und Schwarz, Mühldorfstr. 1, D-81614 München, Germany.

[1] E. Goldobin, H. Kohlstedt, and A.V. Ustinov, Appl. Phys. Lett. **68**, 250 (1996).
[2] W. Walkenhorst, G. Hechtfischer, S. Schlötzer, R. Kleiner, and P. Müller, Phys. Rev. B **56**, 8396 (1997).
[3] A.V. Ustinov, Physica D **123**, 315 (1998), and references therein.
[4] N.F. Pedersen and A.V. Ustinov, Supercond. Sci. Technol. **8**, 389 (1995), and references therein.
[5] E. Goldobin, A. Wallraff, N. Thyssen, and A.V. Ustinov, Phys. Rev. B **57**, 130 (1998).
[6] G. Hechtfischer, R. Kleiner, A.V. Ustinov, and P. Müller, Phys. Rev. Lett. **79**, 1365 (1997); G. Hechtfischer, R. Kleiner, A.V. Ustinov, and P. Müller, Appl. Supercond. **5**, 303 (1998).
[7] N. Thyssen, A.V. Ustinov, and H. Kohlstedt, J. Low Temp. Phys. **106**, 201 (1997).
[8] N. Thyssen, Ph.D. thesis, University of Erlangen-Nürnberg, 1999.
[9] R. Kleiner, F. Steinmeyer, G. Kunkel, and P. Müller, Phys. Rev. Lett. **68**, 2394 (1992). For a review, see R. Kleiner and P. Müller, Physica C **293**, 156 (1997).
[10] A. Yurgens, D. Winkler, N.V. Zavaritsky, and T. Claeson, Phys. Rev. B **53**, R8887 (1996).
[11] Yu.I. Latyshev, J.E. Nevelskaya, and P. Monceau, Phys. Rev. Lett. **77**, 932 (1996).
[12] K. Schlenga, W. Biberacher, G. Hechtfischer, R. Kleiner, B. Schey, O. Waldmann, W. Walkenhorst, P. Müller, F.X. Régi, H. Savary, J. Schneck, M. Brinkmann, H. Bach, K. Westerholt, and G. Winkel, Physica C **235**, 3273 (1995).
[13] W. Lawrence and S. Doniach, *Proceedings of the Twelfth International Conference on Low Temperature Physics*, edited by E. Kanda (Academic Press of Japan, Kyoto, 1971), p. 361.
[14] J.R. Clem and M.W. Coffey, Phys. Rev. B **42**, 6209 (1990).
[15] J.R. Clem, M.W. Coffey, and Z. Hao, Phys. Rev. B **44**, 2732 (1991).
[16] M.W. Coffey and J.R. Clem, Phys. Rev. B **44**, 6903 (1991).
[17] L.N. Bulaevskii, M. Zamora, D. Baeriswyl, H. Beck, and J.R. Clem, Phys. Rev. B **50**, 12 831 (1994).
[18] S. Sakai, P. Bodin, and N.F. Pedersen, J. Appl. Phys. **73**, 2411 (1993).
[19] R. Kleiner, P. Müller, H. Kohlstedt, N.F. Pedersen, and S. Sakai, Phys. Rev. B **50**, 3942 (1994).
[20] T. Koyama and M. Tachiki, Phys. Rev. B **54**, 16 183 (1996); M. Machida, T. Koyama, and M. Tachiki, Phys. Rev. Lett. **83**, 4618 (1999).
[21] D.A. Ryndyk, Phys. Rev. Lett. **80**, 3376 (1998).
[22] Ch. Preis, Ch. Helm, J. Keller, A. Sergeev, and R. Kleiner, Proc. SPIE **1998**, 236.
[23] G. Hechtfischer, R. Kleiner, K. Schlenga, W. Walkenhorst, P. Müller, and H.L. Johnson, Phys. Rev. B **55**, 14 638 (1997).
[24] J.U. Lee, J.E. Nordman, and G. Hohenwarter, Appl. Phys. Lett. **67**, 1471 (1995).
[25] N. Mros, V.M. Krasnov, A. Yurgens, D. Winkler, and T. Claeson, Phys. Rev. B **57**, R8135 (1998).
[26] V.M. Krasnov, N. Mros, A. Yurgens, and D. Winkler, Phys. Rev. B **59**, 8463 (1999).
[27] A. Irie, Y. Hirai, and G. Oya, Appl. Phys. Lett. **72**, 2159 (1998).
[28] J.U. Lee, P. Guptasarma, D. Hornbaker, A. El-Kortas, D. Hinks, and K.E. Gray, Appl. Phys. Lett. **71**, 1412 (1997).
[29] S. Sakai, A.V. Ustinov, N. Thyssen, and H. Kohlstedt, Phys. Rev. B **58**, 5777 (1998).
[30] L.N. Bulaevskii, Turk. J. Phys. **20**, 594 (1996).
[31] S. Sakai, A.V. Ustinov, H. Kohlstedt, A. Petraglia, and N.F. Pedersen, Phys. Rev. B **50**, 12 905 (1994).
[32] N.F. Pedersen and S. Sakai, Phys. Rev. B **58**, 2820 (1998).
[33] R. Kleiner, Phys. Rev. B **50**, 6919 (1994).
[34] V.M. Krasnov and D. Winkler, Phys. Rev. B **56**, 9106 (1997).
[35] L.N. Bulaevskii, D. Dominguez, M.P. Maley, A.R. Bishop, and B.I. Ivlev, Phys. Rev. B **53**, 14 601 (1996); L.N. Bulaevskii, D. Dominguez, M.P. Maley, and A.R. Bishop, *ibid.* **55**, 8482 (1997).
[36] M.V. Fistul and G.F. Giuliani, Physica C **230**, 9 (1994).
[37] S.E. Shafranjuk, M. Tachiki, and T. Yamashita, Phys. Rev. B **57**, 13 765 (1998); **57**, 582 (1998); S.E. Shafranjuk and T. Yamashita, *ibid.* **58**, 121 (1998).
[38] M. Machida, T. Koyama, A. Tanaka, and M. Tachiki, cond-mat/9907136 (unpublished).
[39] A.V. Ustinov and S. Sakai, Appl. Phys. Lett. **73**, 686 (1998).
[40] R. Kleiner, T. Gaber, and G. Hechtfischer (unpublished).
[41] V.M. Krasnov and D. Winkler, Phys. Rev. B **60**, 13 179 (1999).
[42] E. Goldobin and A.V. Ustinov, Phys. Rev. B **62**, 1427 (2000).
[43] C. Tesche and J. Clarke, J. Low Temp. Phys. **29**, 301 (1977).
[44] A. Yurgens, D. Winkler, T. Claeson, G. Yang, I.F.G. Parker, and C.E. Gough, Phys. Rev. B **59**, 7196 (1999).
[45] A. Irie and G. Oya, Physica C **293**, 249 (1997).
[46] K. Schlenga, G. Hechtfischer, R. Kleiner, W. Walkenhorst, P. Müller, H.L. Johnson, M. Veith, W. Brodkorb, and E. Steinbeiss, Phys. Rev. Lett. **76**, 4943 (1996).
[47] Ch. Helm, Ch. Preis, F. Forsthofer, J. Keller, K. Schlenga, R. Kleiner, and P. Müller, Phys. Rev. Lett. **79**, 737 (1997).
[48] K. Schlenga, R. Kleiner, G. Hechtfischer, M. Mössle, S. Schmitt, P. Müller, C. Helm, C. Preis, F. Forsthofer, J. Keller, H.L. Johnson, M. Veith, and E. Steinbeiss, Phys. Rev. B **57**, 14 518 (1998).